

SAMPLING OF BIDIRECTIONAL REFLECTANCE FROM MULTIANGULAR HIGH RESOLUTION AIRBORNE IMAGERY

Antero Kukko

Department of Remote Sensing and Photogrammetry
Finnish Geodetic Institute
PO Box 15, FIN-02431 MASALA, FINLAND
Antero.Kukko@fgi.fi

KEYWORDS: Acquisition; Sampling; DEM/DTM; Aerial; High resolution; Multispectral;

ABSTRACT:

The present investigation describes a method for sampling bidirectional reflectance information from multiangular airborne images. The method uses high resolution surface models in the determination of the location of the imaged point on the ground and in the image, and finally the orientation of the measured surface fragment.

Two test sites were imaged with a wide range of azimuth angles at two different times. A high resolution HRSC-A stereo camera was used for image acquisition. Algorithms to reconstruct the image acquisition and retrieve the image samples from the HRSC-A image data, used with GPS and INS data and automatically derived high resolution digital terrain models, were implemented and used to determine the viewing and illumination geometry on the target surface. The image digital number of a sample point was recorded as an uncalibrated reflectance measure. A large number of directionally defined samples and a wide angular range of sample geometry were obtained by taking the surface orientation, extracted from the high resolution digital surface model, into account.

The images were classified in order to aggregate the samples of a certain surface type acquired from the different images. The sampled reflectance data were tested and analysed by investigating the bidirectional reflectance of seven agricultural and forest targets. Angular uncertainty of the data, and other sources of error affecting the data quality were studied.

Directionally defined reflectance data were acquired to assist in future the modelling and correction of bidirectional effects on airborne optical images used in mapping, urban modelling and for establishment of a bidirectional reflectance database. The multiangular image data, the developed sampling methods and the obtained bidirectional dataset proved to be feasible for investigations of the bidirectional effects of natural targets. Airborne imagery, including scanner and frame images, combined with digital surface models permits extensive investigation of the bidirectional reflectance of a wide range of natural objects and large habitats.

1. INTRODUCTION

Viewing and illumination conditions play a critical role in the interpretation of remote sensing and aerial images, e.g. in the processes of change detection, classification and image mosaicking. Most natural surfaces scatter incident radiation anisotropically (Beisl, 2001; Sandmeier et al., 1998). For such surfaces, sufficient description of the reflectance requires knowledge of the full angular distribution and reliable interpretation of remotely sensed data calls for knowledge regarding all possible surface types (Arnold et al. 2002).

Surface anisotropy is usually described in terms of bidirectional reflectance distribution functions (BRDF). These functions formally describe the scattering anisotropy of a certain type of surface dependent on illumination and viewing directions (θ_i , φ_i) and (θ_r , φ_r), namely

$$f_r(\theta_i, \varphi_i, \theta_r, \varphi_r; \lambda) = \frac{dL_r(\theta_i, \varphi_i, \theta_r, \varphi_r; \lambda)}{dE_i(\theta_i, \varphi_i; \lambda)}, \quad (1)$$

where $dE_i = L_i \cos \theta_i d\omega$ and $d\omega = \cos \theta_i d\varphi_i$. (Beisl, 2001; Jensen, 2000; Sandmeier & Itten, 1999.)

Bidirectional effects on an image are more prominent when a large field of view is used, e.g. in aerial photography (Beisl, 2001). Bidirectional effects cause brightness variation in an

image, depending on the sensed surface type and its condition, the geometric properties of sun-viewing conditions, and the wavelength used. The brightness variation reduces the quality of multi-temporal monitoring and classification if the effect is not corrected because the same surface may seem significantly different in brightness in the images acquired with different sun-viewing geometries. Bidirectional effects are the most severe when the images are taken from the direction of incident light and cause a 'hot spot' on the image (Hapke et al., 1996).

Beisl (2001) describes methods for sampling and correcting bidirectional effects in imaging spectrometer data. Hyperspectral data were acquired using an imaging HyMap spectrometer at three different times and with two perpendicular flight directions. Sampling was carried out by aggregating the pixels representing similar surfaces. This approach improved the angular sampling, which was initially poor.

Airborne Cloud Absorption Radiometer (CAR) has been used extensively in to retrieve the surface reflectance of various types of land cover such as forested wetland and desert (Soulen et al., 2000), cerrado and dense forest (Tsay et al., 1998), and sea ice and tundra (Arnold et al., 2002). In these studies, clockwise circular flight tracks were used in data acquisition over homogenous targets.

Pellikka (1998) uses video images for natural resource assessment. Correction methods were developed for bidirectional effects on video images acquired with a multiangular video system. Separate video frames were

corrected for bidirectional effects using sampled image digital numbers for known natural objects (e.g. alpine meadows and deciduous forests). Multiple video frames produced different measuring geometries. The correction was performed as a function of the scattering angle between instantaneous illumination and measuring directions. The same method was also applied to reduce bidirectional effects in aerial CIR imagery taken on deciduous forest (Pellikka et al., 2000).

The present study aims to find an applicable method interposing field-based goniometry and satellite-based BRDF observations. Goniometry is most capable for fine and tiny objects, such as sand grains, snow, grass, and tree branches, while it is practically impossible to measure a whole tree. The resolution of satellite systems is often too coarse to distinguish fragmented natural objects, but is adequate for large homogenous areas. For instance in Finland, forests and farmlands are generally fragmented into relatively small units and large homogenous areas are a rarity. This may lead to a large number of mixed pixels, reducing the applicability of low-resolution instruments and emphasising the need for a high-resolution airborne measuring system. Also, mosaicking aerial images for the production of three-dimensional models requires techniques that are scientifically well-proven.

The objective of the study was to acquire directionally defined reflectance data to be used in modelling and correction of bidirectional effects on images and for establishment of a BRDF database. This paper presents the detailed calculation of geometric quantities of surface bidirectional reflectance. The accuracy assessment and first tests for the data are presented in the last part of the paper.

2. METHODS

2.1 Test sites

Multiangular images were acquired from two different test sites in southern Finland. The Sjökuulla test site, approximately 1 km² in area, consists mainly of agricultural targets, e.g. barley, wheat and oat fields, meadows and fallow and the forests in the area are mainly broad-leaved trees such as birch and aspen, although there are also coniferous trees such as pine and spruce, with pine being the dominant species. The Finnish Geodetic Institute also has a photogrammetric test field used for calibration of aerial cameras at the test site. The Kuckuberg test site is mainly covered with forests, with some hay and oat fields. The forests are largely old coniferous forests, although there are also some harvested and young areas with deciduous trees and coniferous saplings. The intensive area of the test site was somewhat larger than that of the Sjökuulla area. Both are roughly limited to the intersection area of the intersecting flight strips. The terrain in both areas is slightly contoured. The mean terrain height is about 40 metres above sea level.

2.2 HRSC-A data

A digital HRSC-A stereo camera was used for multiangular image data acquisition. An HRSC-A camera measures with nine different angles ($\pm 18.9^\circ$, $\pm 15.9^\circ$, $\pm 12.7^\circ$, $\pm 3.4^\circ$ and 0.08°) in the flight direction, producing the same number of overlapping image strips. Five spectral bands in visible and near infrared regions are arranged by mounting specific filters for the CCD line sensors. The remaining channels function in a panchromatic band of 585 to 765 nanometres. The radiometric resolution of the HRSC-A was originally 10 bits, which was reduced to eight

bits for the images. More details in table 1 and in (Wewel et al., 2000.)

Focal length	175 mm
Field of view	37.8°×11.8°
Number of CCD sensor lines	9
CCD-sensors per line	5184 (active)
Size of sensor cell	7 μm
Radiometric resolution	10 bit, reduced to 8 bit
Spectral bands:	
Panchromatic	585-765 nm
Blue	395-485 nm
Green	485-575 nm
Red	730-770 nm
Near infrared	925-1015 nm

Table 1. Technical parameters of the HRSC-A.

The spatial resolution of the images used for sampling was interpolated to 0.5 metres for CIR images and 0.3 metres for panchromatic stereo bands. Images were projected to UTM zone 35 with a central meridian of 27°.

2.3 FGI's HRSC-A flight mission and data acquisition

The HRSC-A flight mission was carried out during a three-day period from 27 to 29 July 2001. Two different acquisition times and four different flight directions were used for both test sites to achieve representative angular range for the image-based sampling of the bidirectional reflectance. First, three parallel flight strips were flown with approximately 40% overlap. Then the flight direction was adjusted approximately 30° clockwise and three parallel lines were again acquired. Four different flight directions were used in every session (see Figure 1). At both test sites image acquisition was carried out twice to obtain sufficient change in illumination due to the sun's movement. As a result, 24 image strips were attained for both test sites. In the Kuckuberg area, the second flight headings of the strips were redirected counter-clockwise.



Figure 1. Image acquisition principle.

The position and orientation data were provided by the GPS-INS system. The position of the camera was recorded and delivered at a second rate, whereas the attitude of the camera was provided with a 10 Hz rate. The position data were at first interpolated linearly to the same rate as that of the attitude data, and the data were combined. Finally, the position and attitude data were interpolated to a frequency of 100 Hz.

2.4 Digital surface model and slope and aspect models

The HRSC-A images were processed automatically by DLR (German Aerospace Center) in the photogrammetric processing described by Wewel et al. (2000). This process permits production of a digital surface model (DSM) of the imaged area. Two raster models for both test sites were produced, one per flight session, with a one-metre cell size. The height resolution of these models was five centimetres. The slope and aspect raster images were calculated to characterise the surface slanting and derive a surface normal for each pixel. The spatial resolution of these models was one metre.

2.5 Sun angle data

The sun angles at the time of image acquisition were determined using time averages for each image strip. A feasibility point near the crossings of the flight strips at both test sites was used. At the Sjöskulla test site, the feasibility point was located at 60° 14' 31.07''N, 24° 23' 3.00''E. In Kuckuberg, the corresponding point was located at 60° 12' 30''N, 24° 27' 00''E.

Sun angles were calculated at one-minute intervals. Angles for the full minute nearest to the average time of an image strip were chosen. The rounding causes some error in the sun direction at the ends of each image strip, but due to the short image acquisition period of a single strip and the even smaller intensive test area this does not have a significant effect. The estimated azimuth error was 0.30° and the zenith angle error 0.06° at the ends of each image strip.

2.6 Ground data

The test sites were examined for ground truth data at the time of the HRSC-A flights. Documentation of the scenes was performed by photographing the targets, determining the species and defining the areas on a map. Vegetation and the current state of growth were also recorded.

For sensor calibration, three additional known reference targets were spread over the area of the photogrammetric test field, which has dark gabbro gravel as background. The reflectance properties of the reference targets have been determined by laboratory calibration tests and they will be used for sensor calibration.

2.7 Sample point determination

To derive a proper reflectance sample with correct angular measures, the image acquisition had to be reconstructed. Using the position and attitude data of the camera and single optics camera model, any image cell on a CCD line sensor could be captured with the known viewing azimuth and zenith angles, and the corresponding target point on the ground surface.

An HRSC-A camera has nine parallel CCD line sensors mounted with specific measuring angles with an 11.8° swath and the location of a sensor cell could be determined using these angles. The height reference surface could be reached by means of a rotation of the constructed image vector with a 3D rotation matrix and by scaling the result

$$\begin{bmatrix} X \\ Y \\ Z \end{bmatrix} = M R_{\kappa} R_{\varphi} R_{\omega} \begin{bmatrix} x \\ y \\ z \end{bmatrix}, \quad (2)$$

where x , y and z are sensor cell coordinates on the image plane and the triplet X , Y , Z is a vector from the projection centre of the camera to the ground. M is the scale factor.

The actual sample point (measured by the camera) was determined by finding the intersection of the target vector and the digital surface model. This was carried out using a bisecting algorithm. The search area for the intersection point in the direction defined by the direction vector was initialised to begin from the maximum height of the surface model and to end at the minimum height of the surface model.

The intersection point lies between these two preset end points. The search for the intersection point was carried out bisecting the search area, or vector, and checking whether the middle point is above or under the surface. If it is above the surface, the beginning of the new search area is set. Otherwise, it is set to be the end of the search area. Iteration continues until the distance between the height surface and iterated point is less than a preset threshold.

The threshold value used in this study was five centimetres, which corresponds to the height resolution of the digital surface models. For a maximum HRSC-A view zenith angle of 18.9°, five centimetres threshold means less than two centimetres uncertainty on the horizontal ground plane, which is acceptable for even more detailed image resolution.

The 11.8° opening angle of a single line sensor was divided into 200 parts, giving an angular separation of 0.059° for adjacent samples. This corresponds to a distance of approximately 3 metres between the sampled data points in a cross-track (i.e. sensor) direction from a flight altitude of 3000 metres. In flight direction, the sampling interval was approximately 3.5 metres at flight a speed of 69 m/s and was attained by linearly interpolating the sparse one second interval GPS data and 1/10 second interval inertia data to a 1/100 second interval dataset and picking every fifth point with its position and attitude data from the set. Linear densification is considered to have only a minor effect on data quality.

2.8 Geometric measures of BRDF: flat and slanting surfaces

The BRDF geometry was first investigated for a flat surface. The view zenith angle of a sample was calculated simply, using the target and zenith vectors. The azimuth of the target vector was measured clockwise from the north. Sun angles were calculated as described above in caption 2.5 and were applied here. The relative azimuth of the viewing and illumination directions was calculated.

Regarding each DSM point as a slanting plane, the BRDF coordinates could be determined in relation to the normal vector of this plane. The aspect value was corrected for meridian convergence and the normal \vec{n} was constructed out of the corresponding slope and aspect values of the sampled object point. Sun and viewing vectors \vec{s} and \vec{c} were constructed using the corresponding zenith and azimuth values (θ_{i0} , φ_{i0} and θ_{r0} , φ_{r0}). Viewing and illumination zenith angles θ_r and θ_i relative to the surface normal were then calculated.

The relative azimuth of viewing and illumination directions was determined on the slanting plane and vectors were thus projected onto that plane. Point $P_0 \hat{=} \bar{r}_0$ and surface normal \bar{n} uniquely define a plane in E^3 space; point $P \hat{=} \bar{r}$ lies on this plane if and only if

$$\bar{n} \cdot (\bar{r} - \bar{r}_0) = 0. \quad (3a)$$

Written in three-dimensional coordinates, the plane equation becomes

$$n_1x + n_2y + n_3z = \bar{n} \cdot \bar{r}_0 = d, \quad (3b)$$

where n_i are the components of the surface normal.

By setting $\bar{r}_0 = \bar{0}$, the plane origin equals the origin of E^3 . Let us relocate the surface normal and viewing and illumination vectors to this origin. Thus $d=0$ in equation (3b), because \bar{r}_0 is now perpendicular to any vector lying on the plane. Projections of vectors \bar{s} and \bar{c} on xy-plane are denoted by \tilde{s} and \tilde{c} and are derived by setting the third coordinate of \bar{s} and \bar{c} to zero. Projections \hat{s} and \hat{c} on an arbitrary surface can be derived by solving the following equation

$$z = \frac{-n_1x - n_2y}{n_3}, n_3 \neq 0, \quad (4)$$

where x and y are first two components of vector \tilde{s} or \tilde{c} . The relative azimuth of viewing and illumination directions on an arbitrary surface is then calculated.

2.9 Atmospheric effects

Atmospheric influence on electromagnetic radiation is a severe obstacle to remote sensing. In image analysis and interpretation of aerial images, one typically has difficulties due to the different effects caused by atmospheric scattering and weather conditions (Widen, 1999). The atmosphere has an influence on the measured signal comparable to the BRDF effect on the ground (Beisl, 2001) and can drastically alter the spectral nature of the radiation at-sensor level (Schowengerdt, 1997). Atmospheric effects must therefore be eliminated before any analysis (Beisl, 2001).

The atmospheric influence on HRSC-A images was reduced by estimating the atmospheric parameters from the images themselves. The dark object subtraction (DOS) was chosen as a method for correcting of the images for atmospheric effects. This method focuses on estimating the upwelling atmospheric path radiance, with the view path transmittance assumed to be one. This assumption is reasonable enough, since the path radiance is the most dominant atmospheric effect in the visible spectral region (Schowengerdt, 1997). The use of DOS, as documented, does not hinder application of more developed methods such as ATCOR (Richter, 2000) for later atmospheric correction of sampled data.

DOS coefficients were determined for each image strip by histogram analysis. The DOS coefficient of an image was first set at zero and then incremented stepwise by one. Pixels representing the current value were inspected, and if they were acceptable as a dark object, the coefficient was incremented and the evaluation performed again.

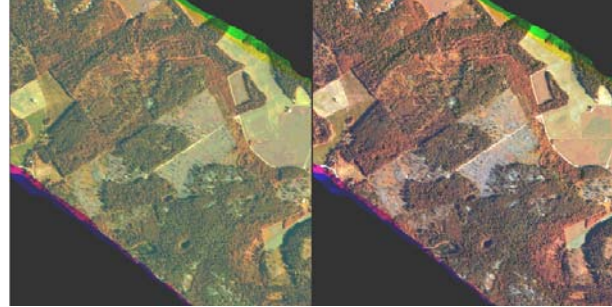


Figure 2. The effect of DOS.

2.10 Classification

A target represented by a single sample point was identified by classifying the images with a maximum likelihood classifier and by manual clustering. DOS-corrected images were fused by constructing four image mosaics for a flight period, one per flying direction. Consequently the sun movements could be taken into account more precisely in the sampling process.

The primary classification was conducted manually, using visual interpretation of the HRSC-A images, maps, terrestrial photographs and field investigations performed at the time of image acquisition. Although some of the classes are not fully identified for species, they are thoroughly clustered. For the Kuckuberg test site, primary classification was performed in a manner similar to that of the Sjöckulla area, but border areas between different class types were left out.

A maximum likelihood classifier was used to construct the secondary classification. Three parallel HRSC-A images and a conducted normalised difference vegetation index (NDVI) were used as input. The initials for image clustering were calculated from statistics on the images using principal axis means. Classification was performed with a 98% convergence threshold.

The secondary classification can be used in data analysis, for instance to distinguish deep shadowed targets from the others. It also provides additional information on internal variation within a target class caused by soil moisture, vegetation closure (sparseness) and other such factors.

3. RESULTS AND DISCUSSION

3.1 Sampling

The image sampling is illustrated in Figure 3. Iteratively solved samples are shown on top of a sampled image strip (50 points per line). The residual for viewing direction was 0.2° . This is considered to be reasonable and acceptable for the determination of bidirectional reflectance. The developed algorithms were found to be efficient and operational for this purpose.



Figure 3. Sample points imposed on a sampled image.

3.2 Bidirectional dataset

As the end product, a large amount of directionally defined data was generated. A single entry in a dataset consists of the following data: sensor id (1-9), camera and sample point locations, slope, aspect, sampled intensity, sensor azimuth, nominal measuring angle, sun azimuth, sun zenith angle, measuring azimuth, measuring zenith angle, relative azimuth (sun-camera), brdf azimuth, brdf zenith angle, sun azimuth and sun zenith angle relative to surface normal, measuring azimuth and measuring zenith angle relative to surface normal, relative azimuth using the inclined surface and finally the primary and secondary classes according to the corresponding classifications.

The total amount of data was 4.3Gbytes of ASCII files named according to date, the sensor bandwidth, and the flight strip number. The wavelength range of the data extends from 395 to 1015 nanometres and the radiometric resolution of the data is 8 bits.

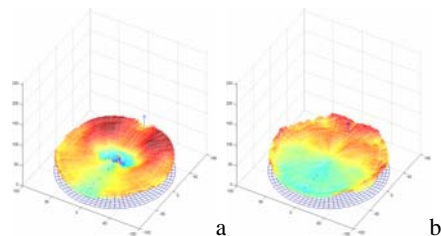


Figure 4. Bidirectional effect for (a) pine and (b) spruce copse using the HRSC-A based data set. Surface normalised sun zenith in (a) 90° and in (b) 60° (blue circle).

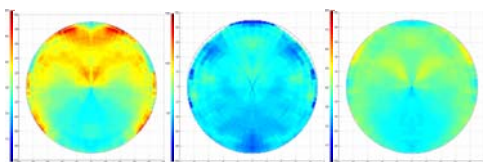


Figure 5. Grey level variation of spruce, birch and pine as function of viewing angle. Sun zenith angle 50 degrees.

In figures 4 and 5, some of the sampled target reflectance anisotropy are presented. In these presentations the surface compensated BRDF is used, an eight bit image DN as a anisotropy unit. Presentations show potential of providing additional information for tree species determination.

3.3 Analysis of accuracy

Because of the short image acquisition period of a single strip, the sun movements during the image acquisition can be considered to be constant. Due to this assumption and the distance from the feasibility point used in sun angle calculations the maximum azimuth error was estimated to be 0.30° and the zenith angle error to be 0.06° at the both ends of an image strip. For the selected intensive areas errors are obviously smaller.

The accuracy of the viewing direction is a function of the accuracy of the attitude data of the sensor. Sensor attitude was systematically corrected, based on empirical measures, on an average of 0.80° for pitch and 0.20° for yaw, most likely due to the map projection. The need could not be specified exactly, however, and must thus be included as a source of uncertainty in the data. The linear densification of the positioning and attitude data adds some minor uncertainty to the viewing direction. This is considered to lie within acceptable limits relative to the imaginable range of applications using the data.

The surface normal direction is more problematic. The angular behaviour of the calculated slope and aspect layers were studied using surface normal vectors for the two sequential digital surface models. Surface normal vectors were constructed at each point and the angular difference was calculated. In Figure 6, this difference is represented by means of a raster image. The calculated mean difference was 9.2° and the standard deviation 15.1°. At maximum, the obtained angular difference was 164.8° for some forest pixels.

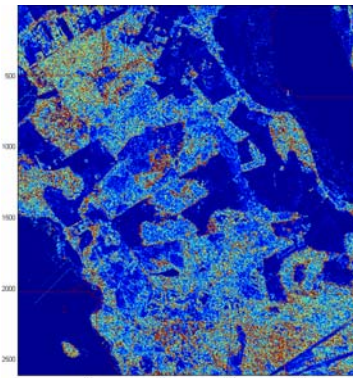


Figure 6. Surface normal uncertainty.

The surface normal uncertainty is mainly caused by the smoothness of the terrain models, e.g. the model fills in small gaps between trees and other structures. The edges between forests and low vegetation seems also to be problematic.

The angular variability was most prominent in forested areas, while for farmlands and water areas it was much smaller. This is due both to mutual occlusion and shadowing of trees, which affect the DSM processing, and to the automatic-image-based DSM creation itself. The spatial and height resolutions of the DSM also play a role in this behaviour.

4. CONCLUSIONS

In this study, multi angular HRSC-A images and digital surface models were used in examination of bidirectional reflectance from multi angular high-resolution HRSC-A images. Method uses high-resolution DSM to approximate the orientation of the

surface of the objects. Position and orientation data were utilized to determine the viewing and illumination geometry relative to the object surfaces. Classification and field investigations were used to identify and delineate the sampled natural and built objects. Algorithms for reconstructing the image acquisition and retrieving image samples with known geometry were developed, implemented and tested.

Directionally defined reflectance data were acquired to be used in correction for bidirectional effects on aerial images and for establishment of a bidirectional reflectance database.

First experiments of the data show the potential of the method in the extraction of reflectance information from digital multi angular images. The use of high-resolution surface models for this purpose gives an interesting opportunity to investigate large objects in a detailed manner. If well defined, the objects under study will even be processed one by one and the data gathered from multiple instances of a same type of object can be combined in a convenient manner.

Data also demonstrate the potential of using the bidirectional data in the extraction of tree species information; i.e. the 3D presentations for each of the species differ significantly from each other and the within species variation due to changes in viewing and sun angles is prominent (see figure 5). Thus, it seems that for example the tree species can be determined more reliable by using multi-angular measurements.

The most remarkable angular uncertainty cumulates from the digital surface models. The accuracy of the surface orientation may be improved by replacing the image-based DSM with a surface model derived using a high density LIDAR data (Hyypä et al., 2001; Kraus & Pfeifer, 1998; Pyysalo, 2000). This could provide more detailed and precise surfaces for BRDF sampling purposes. Also, improving the spatial and height resolution of the surface models to a corresponding image resolution or even better would be worth considering.

REFERENCES

Arnold, G. T., Tsay, S.-C., King, M. D., Li, J. Y. & P. F. Soulen, 2002. Airborne spectral measurements of surface-atmosphere anisotropy for arctic sea ice and tundra. *International Journal of Remote Sensing*, 23 (18), 3763-3781.

Beisl, U., 2001. Correction of Bidirectional Effects in Imaging Spectrometer Data. *Remote Sensing Series 37* – Zurich: Remote Sensing Laboratories. ISBN 3-03703-001-1.

Hapke, B., DiMucci, D., Nelson, R. & W. Smythe, 1996. The cause of the hot spot in vegetation canopies and soils; shadow-hiding versus coherent backscatter. *Remote Sensing of Environment*, 58, 63-68.

Hyypä, J., Schardt, M., Haggrén, H., Koch, B., Lohr, U., Scherrer, H. U., Paananen, R., Luukkonen, H., Ziegler, M., Hyypä, H., Pyysalo, U., Friedländer, H., Uuttera, J., Wagner, S., Inkinen, M., Wimmer, A., Kukko, A., Ahokas, E. & M. Karjalainen, 2001. HIGH-SCAN: The first European-wide attempt to derive single-tree information from laserscanner data. *The Photogrammetric Journal of Finland*, 17 (2), 58-68.

Jensen, J. R. 2000. *Remote sensing of the environment: an earth resource perspective*. Prentice-Hall, USA. ISBN 0-13-489733-1.

Kraus, K. & N. Pfeifer, 1998. Determination of terrain models in wooded areas with airborne laser scanner data. *ISPRS journal of Photogrammetry and Remote Sensing*, 53, 193-203.

Pellikka, P., 1998. Development of correction chain for multispectral airborne video camera data for natural resource assessment. *Fennia*, 176:1, 1-110.

Pellikka, P., King, D. J. & G. Leblanc, 2000. Quantification and reduction of bidirectional effects in aerial CIR imagery of deciduous forest using two reference land surface types. *Remote sensing Reviews*, 19 (1-4), 259-291.

Pyysalo, U., 2000. A method to create a three-dimensional forest model from laser scanner data. *The Photogrammetric Journal of Finland*, 17 (1), 34-42.

Richter, R., 2000. A unified approach to parametric geocoding and atmospheric/topographic correction for wide FOV airborne imagery. Part 2: Atmospheric/topographic correction. *Proceedings of the 2nd EARSel Workshop on Imaging Spectroscopy*, Enschede, The Netherlands, 11-13 July 2000.

Sandmeier, S., Müller, C., Hosgood, B. & G. Andreoli, 1998. Physical Mechanisms in Hyperspectral BRDF Data of Grass and Watergrass. *Remote Sensing of Environment*, 66, 222-233.

Sandmeier, S. & K. Itten, 1999. A field goniometer system (FIGOS) for acquisition of hyperspectral BRDF data. *IEEE Transactions on Geosciences and Remote Sensing*, 37 (2), 978-986.

Showengerdt, R. A. 1997. *Remote sensing, models and methods for image processing*. 2nd ed., Academic Press, San Diego, USA. ISBN 0-12-628981-6.

Soulen, P.F., King, M. D., Tsay, S.-C., Arnold, G. T. & J. Y. Li, 2000. Airborne spectral measurements of surface-atmosphere anisotropy during the SCAR-A, Kuwait oil fire and TARFOX experiments. *Journal of Geophysical Research*, 105 D8, 10203-10218.

Tsay, S.-C., King, M. D., Arnold, G. T. & J. Y. Li, 1998. Airborne spectral measurements of surface anisotropy during SCAR-B. *Journal of Geophysical Research*, 103 D24, 31943-31953.

Wewel, F., Scholten, F. & K. Gwinner, 2000. High Resolution Stereo Camera (HRSC)-Multispectral 3D-Data Acquisition and Photogrammetric Data Processing. *Canadian Journal of Remote Sensing*, 26 (5), 466-474.

Widen, N., 1999. Investigating the BRDF of forest and geometrical calibration of aerial images using digitised colour infrared aerial photographs. *Abstracts of 2nd International Workshop on Multiangular Measurements and Models*. Ispra (VA), Italy.

ACKNOWLEDGEMENTS

The Academy of Finland, Jenny and Antti Wihuri foundation, Finnish National Technology Agency and Foundation of Technology are gratefully acknowledged for financial support.